ESTIMATION OF SIDEFORCE, YAWING MOMENT AND ROLLING MOMENT DERIVATIVES DUE TO RATE OF ROLL FOR COMPLETE AIRCRAFT AT SUBSONIC SPEEDS

1. NOTATION AND UNITS (see Sketch 1.1)

The derivative notation used is that proposed in ARC R&M 3562 (Hopkin, 1970) and described in Item No. 86021. Coefficients and aeronormalised derivatives are evaluated in aerodynamic body axes with origin at the aircraft centre of gravity and with the wing span as the characteristic length. The derivatives Y_p, N_p and L_p are often written as C_{Yp}, C_{np} and C_{lp} in other systems of notation, but attention must be paid to the reference dimensions used. In particular, in forming C_{Yp}, C_{np} and C_{lp} differentiation of C_Y, C_n and C_l may be carried out with respect to $pb/2V$ not pb/V as implied in the Hopkin system. It is also to be noted that a constant datum value of V is employed by Hopkin.

This Item makes use of several other Items which have been produced at different times over a period of many years. Although the nomenclature in these Items is consistent for the important parameters such as stability derivatives, it involves some variation for the less significant parameters. Because of this, and to avoid repetition, the Notation given here is limited to the major quantities appearing in the main text of this Item and to quantities not appearing in other Items. When referred to the method in another Item the user should consult the Notation at the front of that particular Item before carrying out any calculations.

		SI	*British*
A	aspect ratio		
a_1	lift-curve slope	rad^{-1}	rad^{-1}
$(a_1)_{C_L = 0}$	value of a_1 at $C_L = 0$	rad^{-1}	rad^{-1}
b	wing span	m	ft
C_D	drag coefficient, $D/\frac{1}{2}\rho V^2 S$		
C'_D	viscous drag coefficient, $C_D - C_L^2/\pi A$		
C_L	lift coefficient, $L/\frac{1}{2}\rho V^2 S$		
ΔC_{Lf}	lift coefficient increment due to flap deployment		
C_l	rolling moment coefficient, $\mathscr{L}/\frac{1}{2}\rho V^2 Sb$		
C_n	yawing moment coefficient, $\mathscr{N}/\frac{1}{2}\rho V^2 Sb$		
C_Y	sideforce coefficient, $Y/\frac{1}{2}\rho V^2 S$		
D	drag	N	lbf
L	lift	N	lbf

$\mathscr{L}$	rolling moment	N m	lbf ft
L_p	rolling moment derivative due to rate of roll, $L_p = (\partial\mathscr{L}/\partial p)/½\rho VSb^2$		
M	Mach number		
$\mathscr{N}$	yawing moment	N m	lbf ft
N_p	yawing moment derivative due to rate of roll, $N_p = (\partial\mathscr{N}/\partial p)/½\rho VSb^2$		
p	rate of roll	rad/s	rad/s
S	wing planform (reference) area	m^2	ft^2
s	wing semi-span	m	ft
V	velocity of aircraft relative to air	m/s	ft/s
v	sideslip velocity	m/s	ft/s
Y	sideforce	N	lbf
Y_p	sideforce derivative due to rate of roll, $Y_p = (\partial Y/\partial p)/½\rho VSb^2$		
α	angle of attack	degree	degree
β	angle of sideslip	degree	degree
Λ_0	wing leading-edge sweep angle	degree	degree
$\Lambda_{¼}$	wing quarter-chord sweep angle	degree	degree
$\Lambda_{½}$	wing half-chord sweep angle	degree	degree
λ	ratio of wing tip chord to wing centre-line chord		
ρ	density of air	kg/m^3	$slug/ft^3$

Additional symbols

$(\ )_F$	denotes component due to fin
$(\ )_f$	denotes component due to trailing-edge flap deployment at constant C_L
$(\ )_T$	denotes component due to tailplane

$( )_w$ denotes component due to wing planform

$( )_\Gamma$ denotes component due to wing dihedral

$( )_\varepsilon$ denotes component due to wing twist

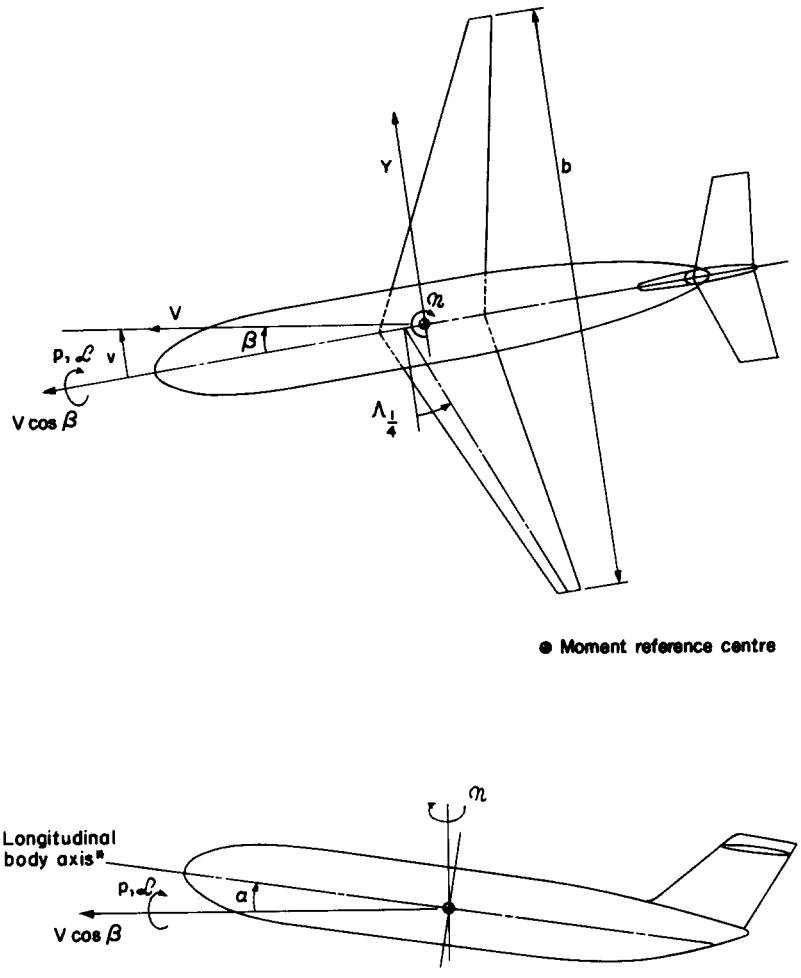

Sketch 1.1 Sign conventions

* The longitudinal body axis is a reference axis fixed in the body in the plane of symmetry. The exact direction of the axis in that plane is conventionally determined by considerations of mid-body geometry.

2. INTRODUCTION

An aircraft's sideforce, yawing moment and rolling moment derivatives due to rate of roll, Y_p, N_p and L_p are normally estimated by calculating the individual contributions of the major components of the aircraft and adding together the part derivatives so obtained. For aircraft at subsonic speeds, separate Items on the various part derivatives have been issued over a number of years. This Item demonstrates how the methods in those separate Items may be combined and illustrates the overall accuracy of prediction by comparing estimated values with wind-tunnel and flight-test data for complete configurations.

Table 2.1 lists the major components of Y_p, N_p and L_p and the Items from which they may be estimated. The total values of the derivatives are obtained by evaluating each component at the same angle of attack and summing the results.

For Y_p the dihedral contribution is important at low α and C_L, because the wing planform and fin contributions are then small and the magnitude of $(Y_p)_\Gamma$ is large and sufficient to determine the sign of Y_p. As α and C_L increase the dihedral contribution remains constant but the planform and fin contributions become increasingly important.

The derivative N_p is determined mainly by the wing planform and fin contributions. The dihedral contribution is very small, and is insignificant except at low α and C_L when the planform and fin contributions are also small.

In general L_p is completely dominated by the wing planform contribution and for a rapid estimate it is sufficient only to calculate $(L_p)_w$.

Comparisons between experimental and predicted values of the rate of roll derivatives are discussed in Section 3. The Derivation is given in Section 4. Section 5 contains a detailed worked example that demonstrates the calculation of the component parts of the derivatives for a particular aircraft and their subsequent combination. The chosen aircraft is that used to demonstrate the calculation of lateral stability derivatives due to sideslip in Item Nos. 81032 (Derivation 38) and 82011 (Derivation 39) and those due to rate of yaw in Item No. 84002 (Derivation 41).

In Section 5 a separate subsection is devoted to the estimation of each major component. Because each subsection contains information and guidance that is additional to that contained in the basic Items listed in Table 2.1, it is useful to refer to the appropriate one when using those Items. In particular a correction for $(L_p)_w$ at high C_L is given in Section 5.3.2.

TABLE 2.1

Component	*Due to*	*Calculated from Item No.*
$(Y_p)_w$, $(N_p)_w$	Wing planform	81014[37]
$(L_p)_w$	Wing planform	Aero A.06.01.01[31]
$(Y_p)_\Gamma$, $(N_p)_\Gamma$, $(L_p)_\Gamma$	Wing dihedral	85006[42]
$(Y_p)_F$, $(N_p)_F$, $(L_p)_F$, $(L_p)_T$	Fin and tailplane	83006[40]
Item Nos Aero A.06.01.00[32] and Aero A.07.01.00[29] give brief introductions to the various components of the yawing and rolling moment stability derivatives. (Derivation numbers are given as indices)		

3. COMPARISONS WITH EXPERIMENT

The wind-tunnel and flight-test data in Derivations 1 to 25 have been used to assess the accuracy of prediction of the derivatives Y_p, N_p and L_p. Data have been studied for a wide variety of aircraft types representing civil transport aircraft, high performance combat aircraft and light and general aviation aircraft, together with results for a number of simpler wind-tunnel models of the type employed to study the effect of systematic variations of geometric parameters. Those data have been taken mostly from low-speed tests of clean-wing configurations with no high-lift devices deployed. Analysis of experimental data for other conditions includes a limited number of results from tests at high subsonic Mach numbers $(M \approx 0.8)$ and a few data from low-speed tests on configurations with leading-edge slats or trailing-edge flaps deployed.

The wind-tunnel data come from two different types of tests. In one, the model is either rolled at a constant rate or is placed in a steady rolling flow, and in the other it is oscillated in roll. The oscillatory system provides a less direct and therefore less precise measurement of the roll rate derivatives. The flight-test data come from tests in which the dynamic response of an aircraft to various control inputs is measured, and the complete set of aerodynamic stability derivatives consistent with that response is deduced. The accuracy with which the various derivatives can be identified by this process depends on the sensitivity of the aircraft to each derivative. Satisfactory estimates are usually possible for the derivatives N_p and L_p, but the response of the aircraft is so insensitive to Y_p that it is usually omitted from the analysis.

3.1 Accuracy of Prediction at Low α and C_L

Comparisons with experimental data have revealed that at low α and C_L, as shown in Sketch 3.1, Y_p is estimated to within about ± 0.06, N_p to within about ± 0.016 and L_p to within about ± 10 per cent. These figures are consistent with the accuracies associated with individual items. As expected the best agreement is achieved with data from rolling model or rolling flow tests. The flight test data show rather more scatter, but the data from tests with oscillatory rigs are subject to the most scatter.

When considering the overall accuracy it is useful to consider Sketches 3.2a to 3.2d that show the predicted component contributions and total values for four different aircraft at cruise conditions.

For the sideforce derivative it can be seen that for the unswept-wing configurations in Sketches 3.2a and 3.2b the dihedral contributions dominate and give negative values of Y_p. The aircraft with swept wings in Sketches 3.2c and 3.2d have more important wing planform contributions that oppose any dihedral contributions and lead to positive values of Y_p. Because the planform and dihedral contributions act in opposite senses any errors in the prediction of either can represent a substantial fraction of the total value.

For the yawing moment derivative Sketches 3.2a to 3.2d show that N_p is comprised of small contributions from the wing planform and dihedral and from the fin. The fin contribution $(N_p)_F$ is particularly difficult to estimate reliably because it is strongly influenced by the wing and body sidewash (see Item No. 83006). Thus the uncertainty in N_p can often be of the same order as its overall magnitude (see Sketch 3.1b).

The situation is much simpler for the rolling moment derivative. In this case the wing planform contribution is completely dominant and the small percentage error in the prediction of L_p corresponds to the basic accuracy associated with the component $(L_p)_w$.

In wholly subsonic flow the effect of Mach number on the rate of roll derivatives is small and predictable, as illustrated in Sketch 3.3.

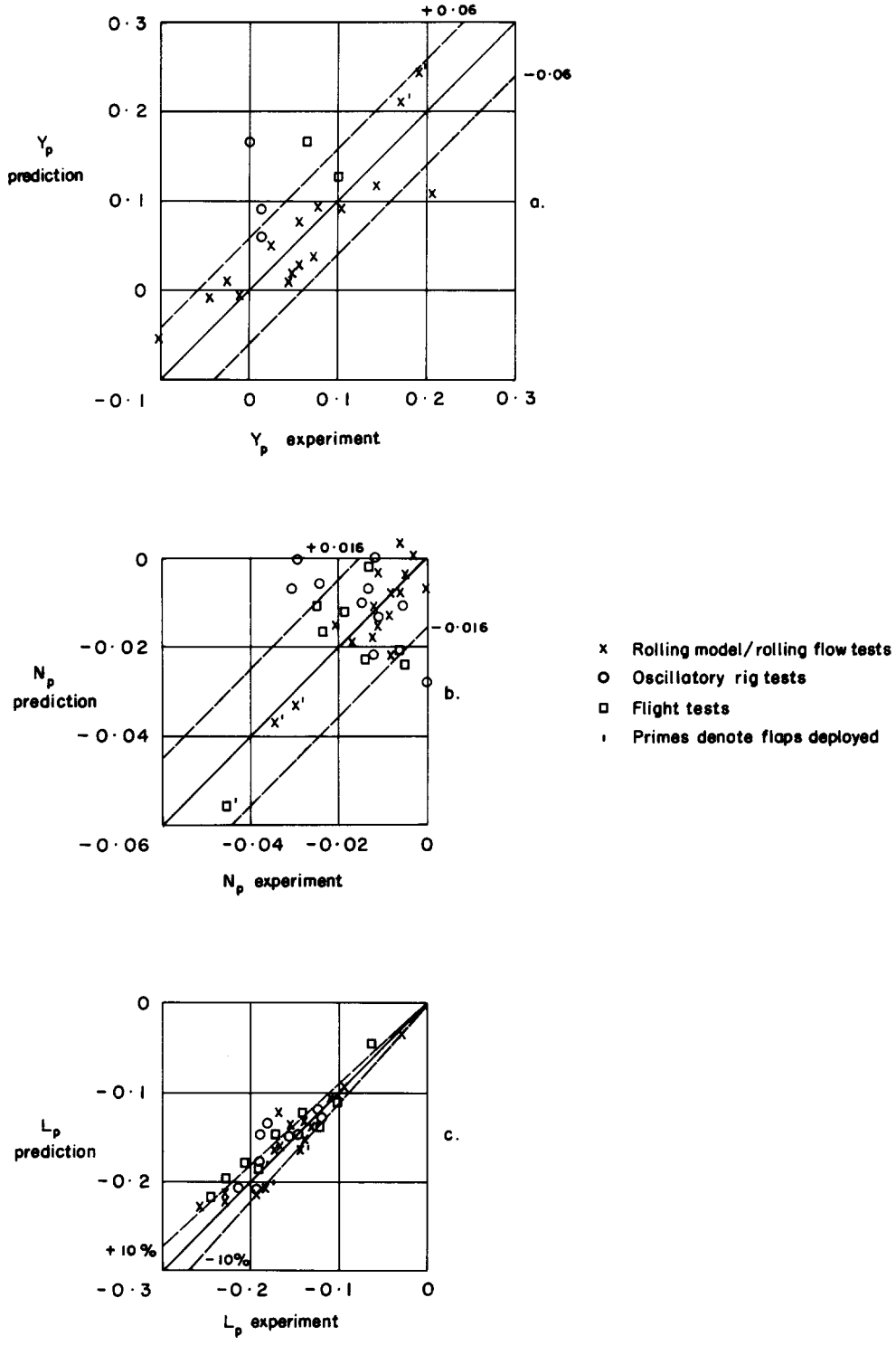

Sketch 3.1 Comparison of predicted values at low α and C_L

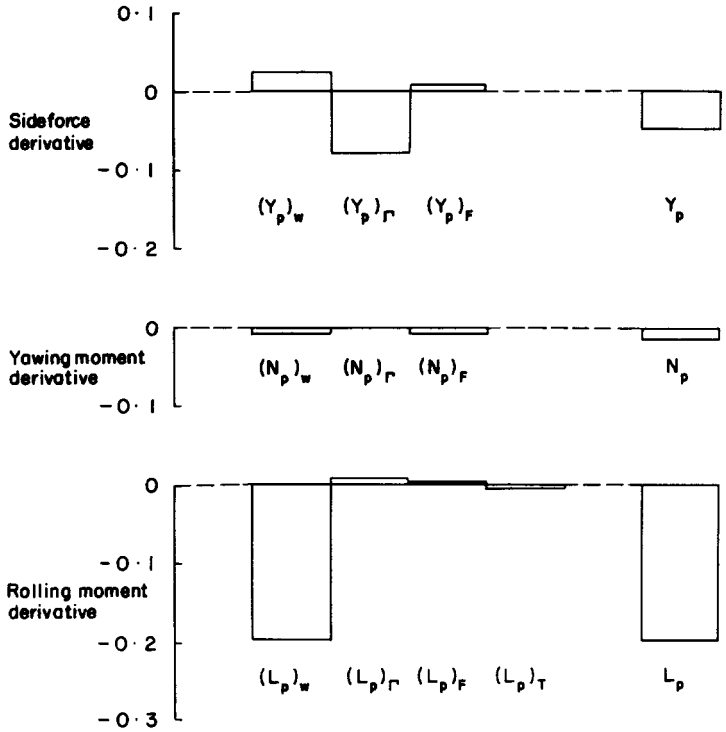

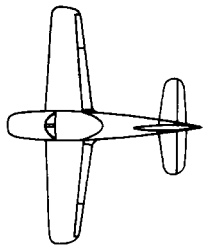

a. Derivations 15 and 16

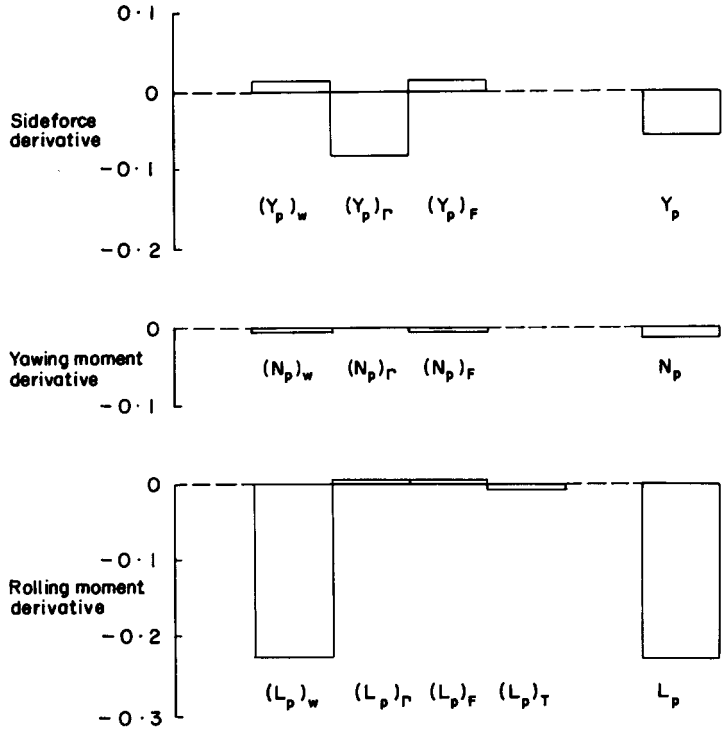

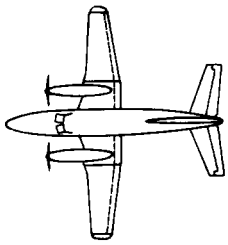

b. Derivation 24

Sketch 3.2 Illustration of component break-down for cruise conditions

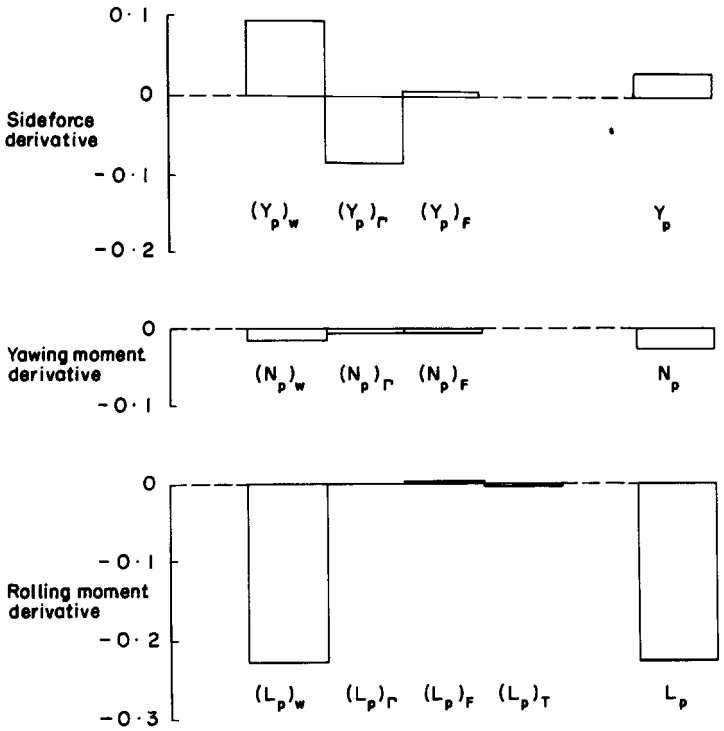

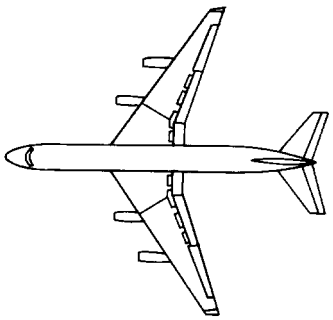

c. Derivations 14 and 17

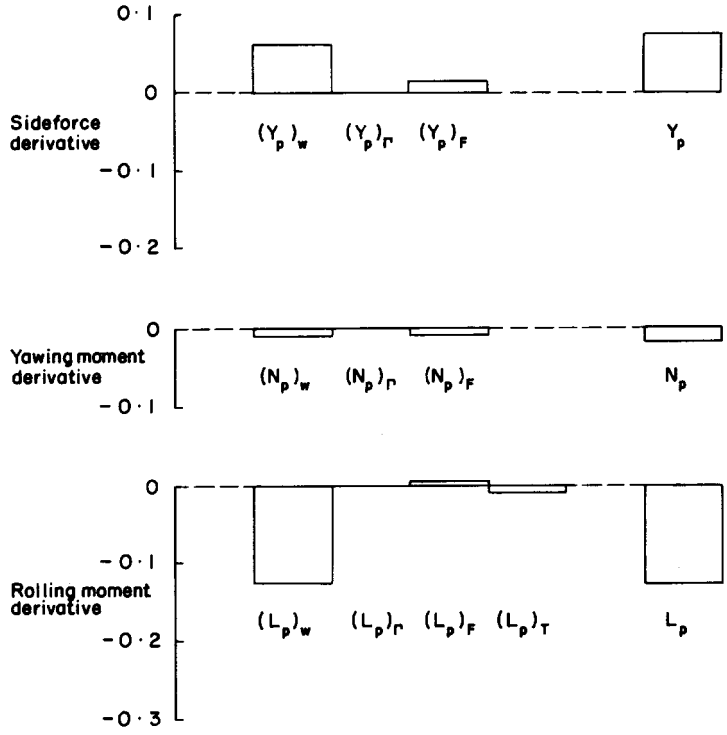

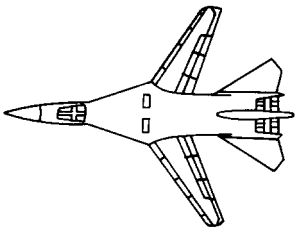

d. Derivation 23

Sketch 3.2 Illustration of component break-down for cruise conditions (concluded)

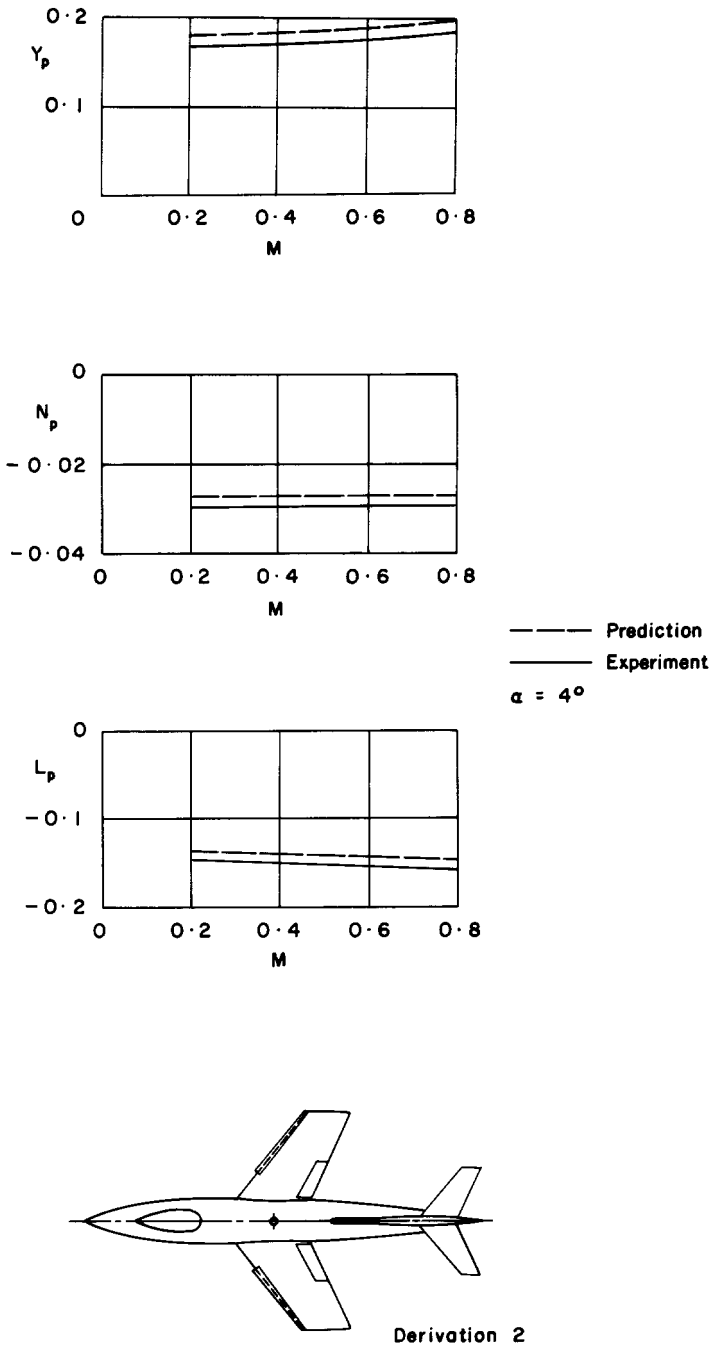

Sketch 3.3 Illustration of variation of derivatives with Mach number

3.2 Variations with α and C_L

3.2.1 General

The accuracy of the prediction of the variation of the rate of roll derivatives with α and C_L cannot be readily quantified and is best illustrated through some typical examples.

It should be remembered that much of the characteristic behaviour of the experimental values of the wing planform contributions to Y_p and N_p is determined by the progressive breakdown of the leading-edge and tip suction forces following the onset of flow separation. Section 3 of Item No. 81014 describes the role of those edge forces with regard to the roll rate derivatives. In brief, the effect is that $(Y_p)_w$ and $(N_p)_w$ increase in magnitude with α until flow separation begins, at which point there is a rapid reduction in the edge forces and hence in the magnitudes of $(Y_p)_w$ and $(N_p)_w$. Eventually $(N_p)_w$, which is initially negative, changes sign and approaches the value $-(L_p)_w \tan\alpha$ that corresponds to a complete absence of edge forces. In Item No. 81014 a method is given for modelling the non-linear behaviour of $(N_p)_w$. This uses the experimental value of the rate of change with angle of attack of the viscous drag coefficient of the wing, *i.e.* $\partial C_D'/\partial\alpha$ where $C_D' = C_D - C_L^2/\pi A$, as a parameter for correlating the flow separation effects. No attempt is made to model the non-linear behaviour of $(Y_p)_w$, which can be expected to fall to zero as the edge forces disappear.

With regard to L_p, the experimental value is almost entirely determined by the wing contribution, and can therefore be expected to remain almost constant with α until flow separation effects influence $(L_p)_w$. Usually there is a large fall in the magnitude of $(L_p)_w$ at high α close to the stall. Item No. Aero A.06.01.01 only provides predictions for attached flow, but in Section 5.3.2 a method for modifying the prediction to allow for flow separation is discussed.

3.2.2 Example 1

Sketch 3.4 compares the total predicted and experimental values of Y_p, N_p and L_p for a model tested in rolling flow, and Sketch 3.5 demonstrates how the total predicted values break down into wing planform and fin contributions.

In Sketch 3.4a it can be seen that the experimental variation of Y_p with α is modelled quite well for $\alpha \leq 4°$. Above that there is poor agreement because no attempt is made to predict the non-linear variation of the wing planform contribution. Sketch 3.5a shows that $(Y_p)_w$ provides the major contribution to Y_p with a smaller contribution of the same sign coming from $(Y_p)_F$.

For N_p, Sketch 3.4b shows that a fairly uniform discrepancy is maintained between the experimental and predicted values for $\alpha \geq 2°$. The agreement gets only slightly worse as α increases. The values of N_p become increasingly negative until $\alpha \approx 4°$, when the decay of edge forces begins. This causes a fall in the magnitude of the wing planform contributions which is mirrored by the decrease in the magnitude of N_p until $\alpha \approx 8°$, after which N_p again assumes increasing negative values due to the growing influence of the fin contribution. Sketch 3.5b illustrates this interplay for the predicted values. Although $(N_p)_w$ changes sign and takes positive values from $\alpha \approx 7°$, the steadily increasing negative contribution $(N_p)_F$ is sufficient to overcome this and determine the ultimate variation of N_p.

For L_p, Sketch 3.4c shows that there is an early fluctuation in the experimental value for $5° \leq \alpha \leq 10°$. This is presumably due to local flow separations. Apart from this the general accuracy of prediction is good up to $\alpha \approx 16°$, after which the predicted and experimental values diverge rapidly as the stall is approached. Sketch 3.5c shows that the predicted value of L_p is almost entirely determined by $(L_p)_w$, but the tiny contribution $(L_p)_F$ adds shape to the curve.

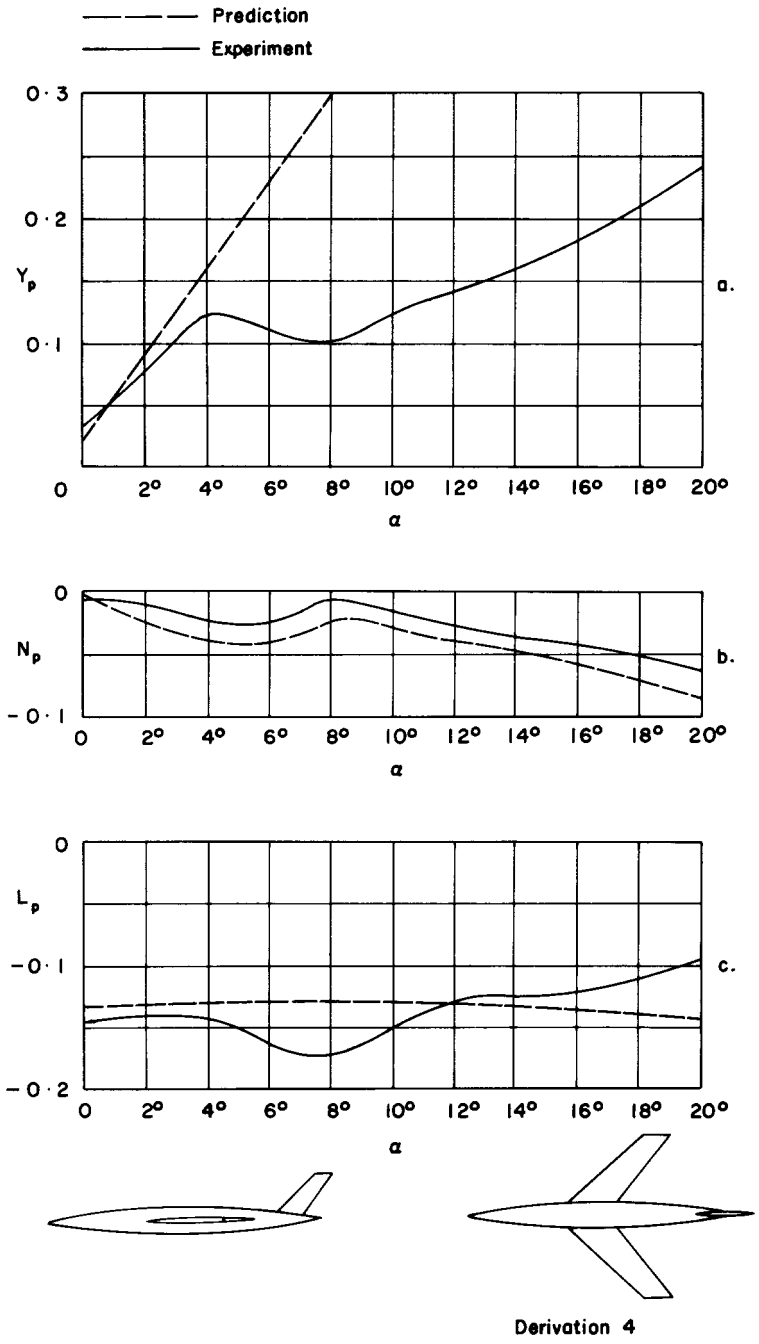

Sketch 3.4 Comparison of predicted and experimental variations with α

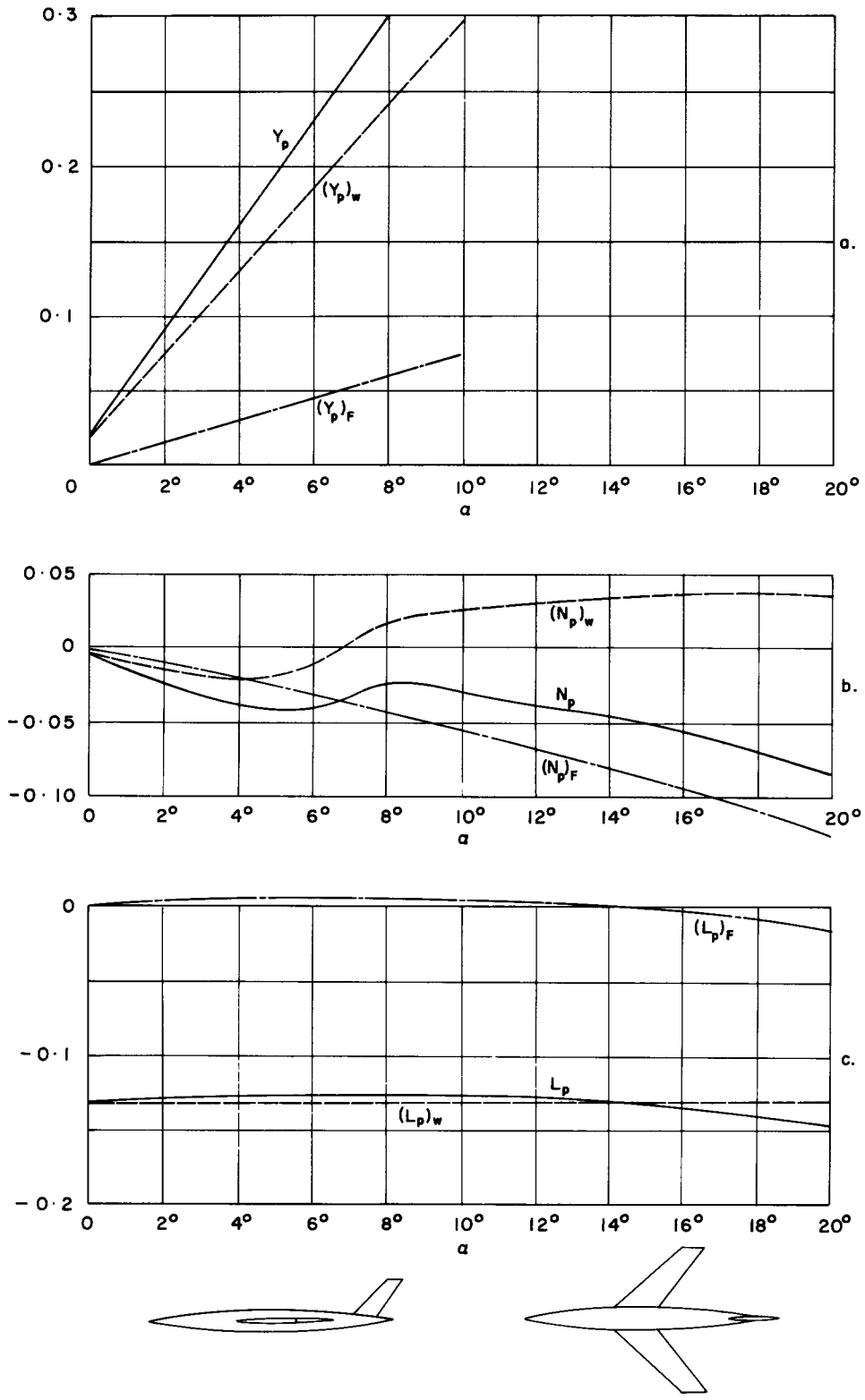

Sketch 3.5 Comparison of wing and fin contributions to total predicted values

3.2.3 Example 2

In Sketch 3.6 the stability derivatives are plotted against C_L for a configuration tested in rolling flow both with a clean wing and in the landing configuration with wing leading-edge slats, trailing-edge flaps and undercarriage deployed. The clean-wing data show many of the same trends as the data in Sketch 3.4. Both the Y_p and N_p experimental curves increase fairly linearly at low C_L and lie close to the predicted values. However, at $C_L \approx 0.3$ both curves break and fall in magnitude. After that no serious attempt is made to predict Y_p. A prediction of N_p has been attempted but, because there are no experimental data on the drag of the wing, only a rough estimate of $\partial C_D'/\partial\alpha$ could be made. Too low an estimate of $\partial C_D'/\partial\alpha$ has resulted in an insufficient reduction in the predicted value of N_p for $0.35 \le C_L \le 0.7$. This highlights the difficulty of predicting the non-linear part of $(N_p)_w$ in the absence of experimental data on lift and drag. For L_p there is again good agreement until the experimental value declines rapidly at high C_L.

The experimental effect of deploying high-lift devices is to delay to a higher C_L the onset of flow separation and therefore to extend the range over which the stability derivatives show nearly linear variations. In Sketch 3.6 it can be seen that predicted values of Y_p are of the correct trend, those for N_p are good and those for L_p remain reasonable.

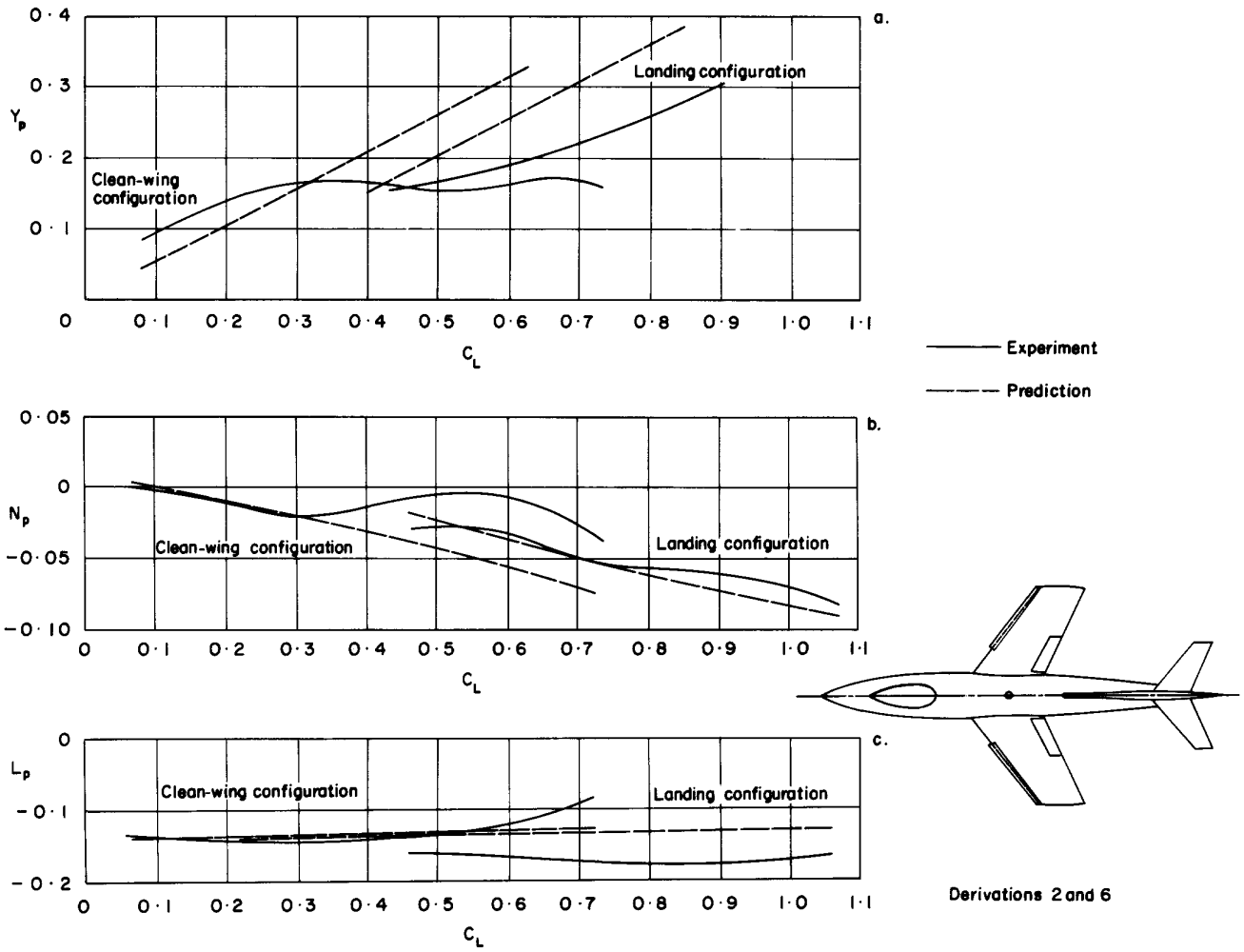

Sketch 3.6 Comparison of predicted and experimental variations with C_L (effect of high-lift devices)

3.2.4 Example 3

In Sketch 3.7 predicted values are compared with flight-test data. The results suggest that N_p and L_p are predicted quite well for wings with low and moderate sweep, but less well for highly swept wings. In general the agreement is very good at low α. The estimate of N_p at higher α would be improved if allowance were to be made for the decay of wing edge forces. An increase in wing sweep reduces the angle of attack at which that decay starts and N_p becomes non-linear. The increase in the magnitude of L_p apparent in the flight-test data for $\Lambda_0 = 58°$ and $\alpha \geq 6°$ is associated with the incremental non-linear lift due to the formation of leading-edge vortices.

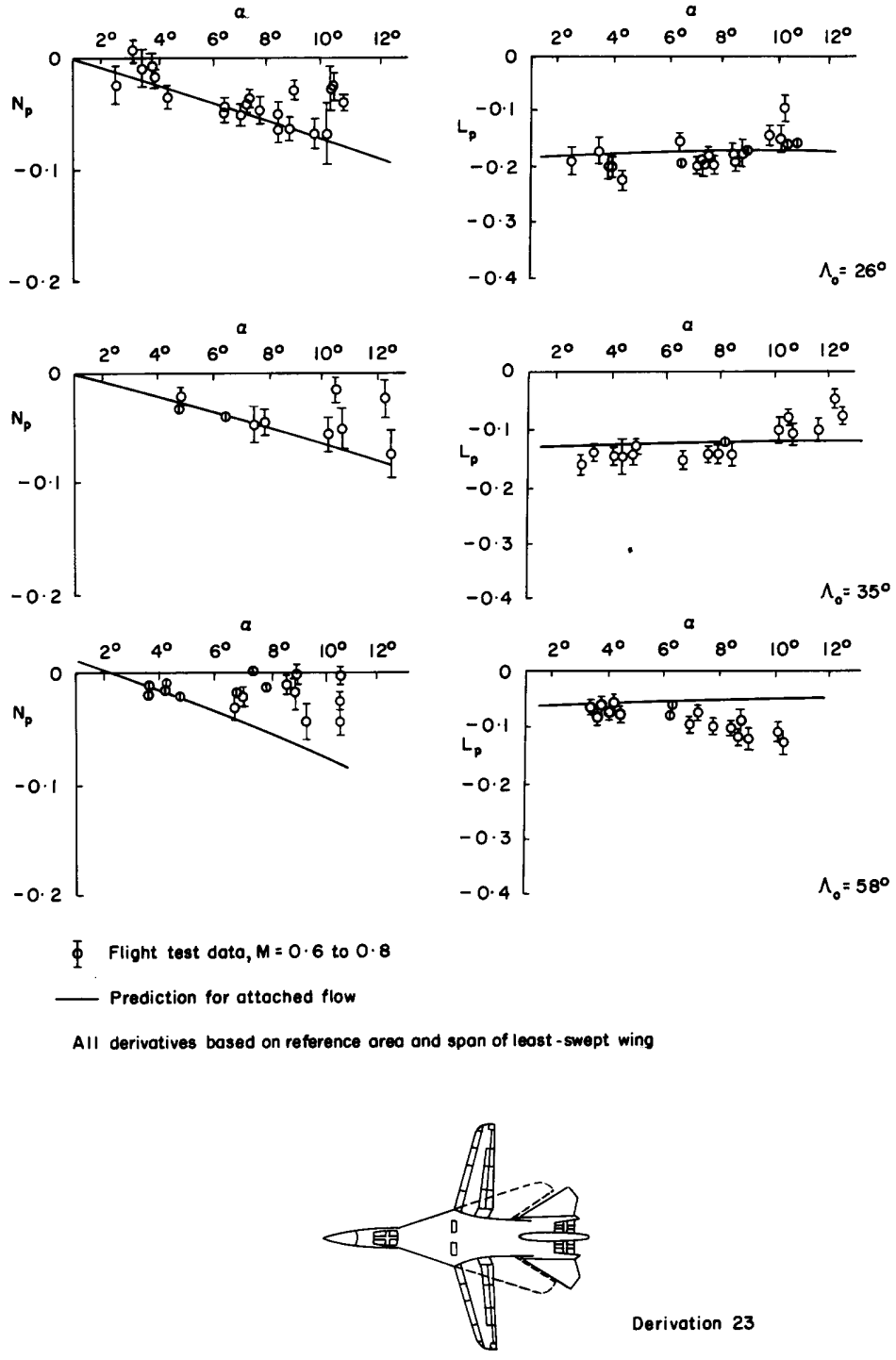

Sketch 3.7 Comparison of predicted and experimental variations with α

4. DERIVATION

The Derivation lists selected sources of information that have assisted in the preparation of this Item.

Experimental Data

1.	BIRD, J.D. LICHTENSTEIN, J.H. JAQUET, B.M.	Investigation of the influence of fuselage and tail surfaces on low-speed static stability and rolling characteristics of a swept-wing model. NACA tech. Note 2741, 1947.
2.	QUEIJO, M.J. GOODMAN, A.	Calculations of the dynamic lateral stability characteristics of the Douglas D-558-II airplane in high-speed flight for various wing loadings and altitudes. NACA RM L50H16a (TIL 3352), 1950.
3.	LETKO, W. RILEY, D.R.	Effect of an unswept wing on the contribution of unswept-tail configurations to the low-speed static- and rolling-stability derivatives of a midwing airplane model. NACA tech. Note 2175, 1950.
4.	WOLHART, W.D.	Influence of wing and fuselage on the vertical-tail contribution to the low-speed rolling derivatives of midwing airplane models with 45° sweptback surfaces. NACA tech. Note 2587, 1951.
5.	BIRD, J.D. JAQUET, B.M.	A study of the use of experimental stability derivatives in the calculation of the lateral disturbed motions of a swept-wing airplane and comparison with flight results. NACA Rep 1031, 1951.
6.	QUEIJO, M.J. WELLS, G.E.	Wind-tunnel investigation of the low-speed static and rotary stability derivatives of a 0.13 scale model of the Douglas D-558-II airplane in the landing configuration. NACA RM L52G07 (TIL 3502), 1952.
7.	WILLIAMS, J.L.	Measured and estimated lateral static and rotary derivatives of a 1/12-scale model of a high-speed fighter airplane with unswept wings. NACA RM L53K09 (TIL 5187), 1954.
8.	FISHER, L.R. LICHTENSTEIN, J.H. WILLIAMS, K.D.	A preliminary investigation of the effects of frequency and amplitude on the rolling derivatives of an unswept-wing model oscillating in roll. NACA tech. Note 3554, 1955.
9.	SLEEMAN, W.C. WIGGINS, J.W.	Experimental investigation at high subsonic speeds of the rolling stability derivatives of a complete model with an aspect ratio - 2.52 wing having an unswept 72 - per cent-chord line and high horizontal tail. NACA RM L54I20 (TIL 6633), 1955.
10.	WOLOWICZ, C.H.	Time-vector determined lateral derivatives of a swept-wing fighter-type airplane with three different vertical tails at Mach numbers between 0.70 and 1.48. NACA RM H56C20 (TIL 6508) 1956.
11.	LOPEZ, A.E. BUELL, D.A. TINLING, B.E.	The static and dynamic rotary stability derivatives at subsonic speeds of an airplane model having wing and tail surfaces swept back 45° . NASA Memo 5-16-59A (TIL 6557), 1959.
12.	HEWES, D.E.	Low-subsonic measurements of the static and oscillatory lateral stability derivatives of a sweptback-wing airplane configuration at angles of attack from –10º to 90º. NASA Memo 5-20-59L (TIL 6506), 1959.

13. HENDERSON, W.P. PHILLIPS, W.P. GAINER, T.G. — Rolling stability derivatives of a variable-sweep tactical fighter model at subsonic and transonic speeds. NASA tech. Note D-3845, 1967.

14. TEPER, G.L. — Aircraft stability and control data. NASA CR-96008, 1969.

15. SECKEL, E. MORRIS, A.J. — The stability derivatives of the Navion aircraft estimated by various methods and derived from flight-test data. Princeton University, Rep. No. FAA-RD-71-6, 1971.

16. SUIT, W.T. — Aerodynamic parameters of the Navion airplane extracted from flight data. NASA tech. Note D-6643, 1972.

17. GILYARD, G.B. — Flight-determined derivatives and dynamic characteristics of the CV-990 airplane. NASA tech. Note D-6777, 1972.

18. PARRISH, R.V. STEINMETZ, G.G. — Lateral stability and control derivatives of a jet fighter airplane extracted from flight test data by utilizing maximum likelihood estimation. NASA tech. Note D-6905, 1972.

19. SUIT, W.T. WILLIAMS, J.L. — Lateral static and dynamic aerodynamic parameters of the Kestrel aircraft (XV-6A) extracted from flight data. NASA tech. Note D-7455, 1974.

20. GRAFTON, S.B. CHAMBERS, J.R. COE, P.L. — Wind-tunnel free-flight investigation of a model of a spin-resistant fighter configuration. NASA tech. Note D-7716, 1974.

21. O'LEARY, C.O. — Wind-tunnel measurements of lateral aerodynamic derivatives using a new oscillatory rig, with results and comparisons for the Gnat aircraft. ARC R&M 3847, 1977.

22. THOMAS, H.H.B.M. — The estimation of lateral-directional aerodynamic derivatives at subsonic speeds. RAE tech. Rep. 77117, 1977.

23. SIM, G.A. CURRY, R.E. — Flight-determined stability and control derivatives for the F-111 TACT research aircraft. NASA tech. Paper 1350, 1978.

24. TANNER, R.R. MONTGOMERY, T.D. — Stability and control derivative estimates obtained from flight data for the Beech 99 aircraft. NASA tech. Memo. 72863, 1979.

25. O'LEARY, C.O. — A comparison of wind-tunnel measurements and estimates of the lateral aerodynamic derivatives of a moderately swept wing transport aircraft. RAE tech. Rep. 83027, 1983.

Methods

26. PINSKER, W.J.G. — Die aerodynamischen Beiwerte der freien Seitenbewegung. DVL UM 1144/1-2, 1943. (DVL UM 1144/1 is translated in Report No. F-TS-619-RE, Air Materiel Command, Wright Field, Dayton, Ohio.)

27. GOODMAN, A. ADAIR, G.H. — Estimation of the damping in roll of wings through the normal flight range of lift coefficient. NACA tech. Note 1924, 1949.

28. CAMPBELL, J.P. McKINNEY, M.O. — Summary of methods for calculating dynamic lateral stability and response and for estimating lateral stability derivatives. NACA Rep. 1098, 1952.

ESDU Items

29. ESDU — Information on the use of Data Items on yawing moment derivatives of an aeroplane. Item No. Aero A.07.01.00, ESDU International, November 1946.

30. ESDU — Lift coefficient increment due to full-span slotted flaps. Item No. Aero F.01.01.08. ESDU International, March 1949.

31. ESDU — Stability derivative L_p rolling moment due to rolling for swept and tapered wings. Item No. Aero A.06.01.01, ESDU International, March 1955.

32. ESDU — Information on the use of Data Items on rolling moment derivatives of an aeroplane. Item No. Aero A.06.01.00, ESDU International, March 1958.

33. ESDU — Lift-curve slope and aerodynamic centre position of wings in inviscid subsonic flow. Item No. 70011, ESDU International, London, July 1970.

34. ESDU — Conversion of lift coefficient increment due to flaps from full span to part span. Item No. 74012, ESDU International, London, July 1974.

35. ESDU — Information on the use of Data Items on flaps including estimation of the effects of fuselage interference. Item No. 75013, ESDU International, London, July 1975. (Superseded by Item Nos 97002 and 97003.)

36. ESDU — Geometric properties of cranked and straight-tapered wing planforms. Item No. 76003, ESDU International, London, January 1976.

37. ESDU — Contribution of wing planform to derivatives of yawing moment and sideforce due to roll rate at subsonic speeds, $(N_p)_w$ and $(Y_p)_w$. Item No. 81014, ESDU International, 1981.

38. ESDU — Estimation of rolling moment derivative due to sideslip for complete aircraft at subsonic speeds. Item No. 81032, ESDU International, 1981.

39. ESDU — Estimation of sideforce and yawing moment derivatives due to sideslip for complete aircraft at subsonic speeds. Item No. 82011, ESDU International, 1982.

40. ESDU — Contribution of fin to sideforce, yawing moment and rolling moment derivatives due to rate of roll, $(Y_p)_F$, $(N_p)_F$, $(L_p)_F$, in the presence of body, wing and tailplane. Item No. 83006, ESDU International, 1983.

41. ESDU — Estimation of sideforce, yawing moment and rolling moment derivatives due to rate of yaw for complete aircraft at subsonic speeds. Item No. 84002, ESDU International, 1984.

42. ESDU — Contribution of wing dihedral to sideforce, yawing moment and rolling moment derivatives due to rate of roll at subsonic speeds, $(Y_p)_\Gamma$, $(N_p)_\Gamma$, and $(L_p)_\Gamma$. Item No. 85006, ESDU International, 1985.

5. EXAMPLE

This section provides a worked example to show how Y_p, N_p, and L_p are calculated for the aircraft dimensioned as shown in Sketch 5.1 together with the additional geometric information in Table 5.1. Both inner and outer flaps are of the single-slotted type. The longitudinal body axis is taken parallel to the mid-body centre-line and passes through the aircraft moment reference centre. Angles of attack, α, are expressed in terms of this axis.

Calculations are performed for two flight conditions:

(i) a cruise condition with $\alpha = 0$, $M = 0.78$ and Reynolds number/metre = 7.5×10^6,

and (ii) a landing condition with $\alpha = 6°$, $M = 0.20$ and Reynolds number/metre = 4.5×10^6.

Where appropriate the components of Y_p, N_p, and L_p are also expressed as functions of α or C_L. The variations of the total values are illustrated by sketches in Section 5.7.

Note that for the aircraft used in this example Item Nos 81032 and 82011 describe the estimation of lateral stability derivatives due to sideslip and Item No. 84002 those due to rate of yaw.

TABLE 5.1 Additional Geometric Parameters for Aircraft in Sketch 5.1

WING		
Angle between wing zero-lift line and longitudinal body axis	3°	
Average section trailing-edge angle	10°	
Average section thickness-to-chord ratio	0.10	
FLAPS (single slotted)	At section FF'	At section GG'
Flap-chord to wing-chord ratio	0.250	0.250
Flap-chord to extended-wing-chord ratio	0.238	0.227
Extended-wing-chord to wing-chord ratio	1.05	1.10
Flap deflection angle	45°	40°
BODY		
Maximum cross-sectional area	28.3 m^2	
Area of side elevation	224 m^2	
FIN		
Side area between tip and root chords	37.8 m^2	

Note (i) The wing and flap section parameters are taken in planes parallel to the aircraft plane of symmetry.

(ii) Boundary-layer transition is assumed to occur at the leading edge of the wing.

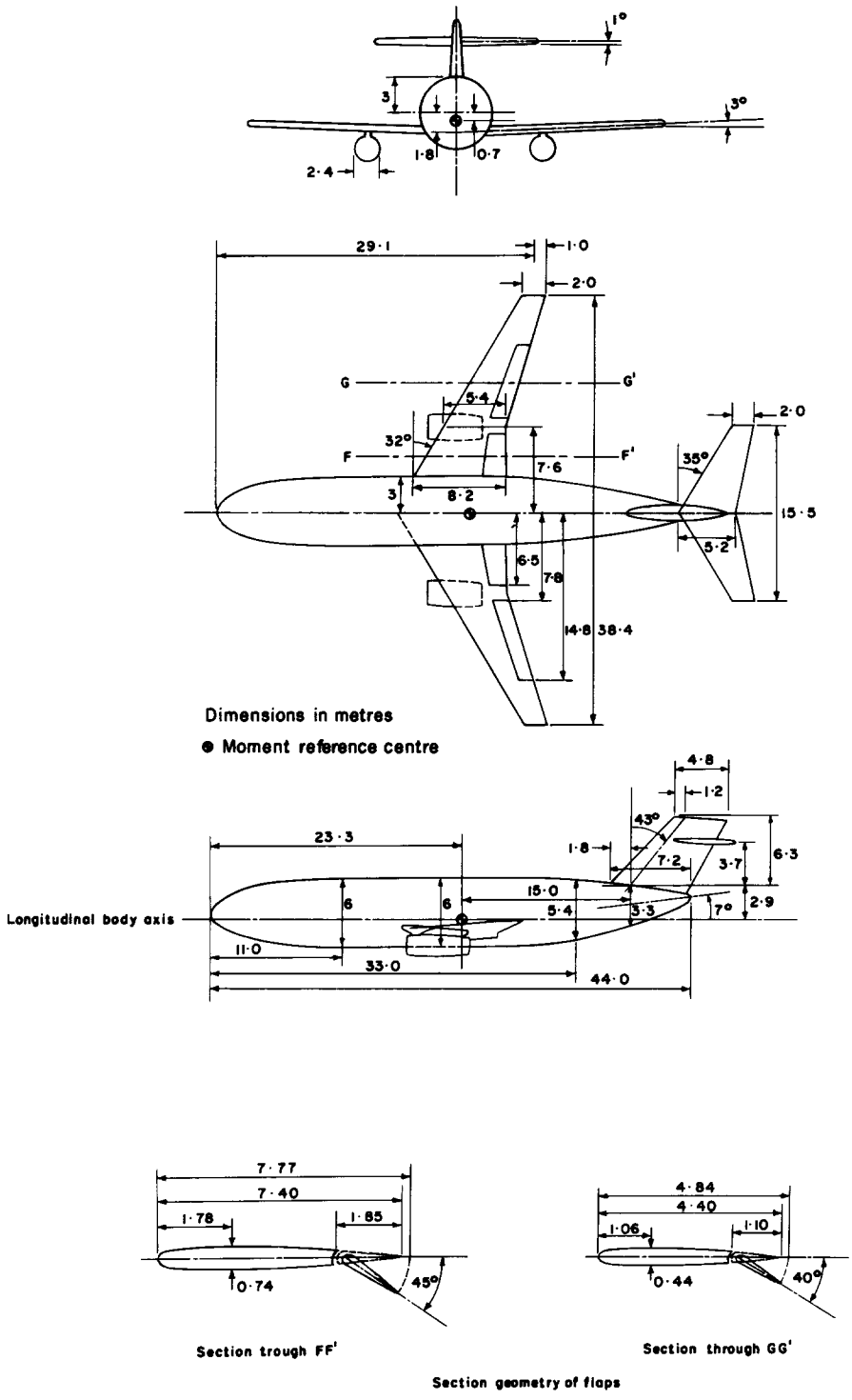

Sketch 5.1 Aircraft geometry

5.1 Calculation of Wing Planform Parameters

See Item No. 76003 for Notation

Before commencing the estimation of Y_p, N_p and L_p it is usually necessary to calculate a number of geometric parameters for the wing planform that are not immediately available from Sketch 5.1 or Table 5.1. This is because the Items dealing with the wing are only directly applicable to straight-tapered wings. Therefore, unless the aircraft has this type of wing, for which the planform parameters can be readily obtained from a scale diagram, a straight-tapered wing equivalent to the true wing has to be constructed by the method in the Addendum to Item No. 76003 (Derivation 36). That Item represents a cranked wing by a straight-tapered wing that has the same span, the same tip chord, and the same exposed wing area outside the intersection of the wing and body planforms, as the true wing. The equivalent-wing planform parameters that result from applying the method in Item No. 76003 to the aircraft in Sketch 5.1 are summarised in Table 5.2.

The values and notation in Table 5.2 are used throughout the example for the wing geometry.

TABLE 5.2 Properties of Equivalent Straight-tapered Wing Planform

Parameter	*Value*	*Parameter*	*Value*
Wing planform area, S	194.3 m^2	Leading-edge sweep, Λ_0	32.0°
Aspect ratio, A	7.59	Quarter-chord sweep, $\Lambda_{¼}$	28.6°
Aerodynamic mean chord, $\bar{\bar{c}}$	5.68 m	Half-chord sweep, $\Lambda_{½}$	25.0°
Ratio of tip chord to root chord, λ	0.246		

5.2 Calculation of Wing and Flap Lift Coefficients

Several of the roll rate derivative components depend on the wing and flap lift coefficients. The estimation of the necessary coefficients is described in Sections 5.2.1 and 5.2.2.

5.2.1 Wing Lift Coefficient, C_L

The wing lift coefficient, C_L, may be estimated by using Item No. 70011 (Derivation 33) to obtain the lift-curve slope (per radian) that is appropriate to the equivalent wing values of $A\tan\Lambda_{½}$, $A(1-M^2)^{½}$ and λ. This is converted to the lift-curve slope per degree and multipled by the angle of attack of the wing, $\alpha+\alpha_w$, where α_w is the angle between the wing zero-lift line and the longitudinal body axis. In this example $\alpha_w = 3°$. For the parameters given in Table 5.2, $\partial C_L/\partial\alpha = 4.48/57.3$ per degree at $M = 0.2$ and $\partial C_L/\partial\alpha = 5.69/57.3$ per degree at $M = 0.78$. See Table 5.3 for a summary of results.

TABLE 5.3 Wing Lift Coefficient

Parameter	*Cruise Condition*	*Landing Condition (flaps retracted)*
α	0	6°
M	0.78	0.20
$A(1-M^2)^{½}$	4.75	7.44
$A\tan\Lambda_{½}$	3.54	3.54
λ	0.246	0.246
$\partial C_L/\partial\alpha$ (per degree)	5.69/57.3	4.48/57.3
$\alpha+\alpha_w$	3°	9°
C_L	0.298	0.704*
C_L (as a function of α)	$0.0993(\alpha+3)$	$0.0782(\alpha+3)$*

* Note this does not include the flap lift increment, see Section 5.2.2.

5.2.2 Flap Lift Coefficient, ΔC_{Lf}

For the single-slotted flaps that are shown in Sketch 5.1, Item No. Aero F.01.01.08 (Derivation 30) can be used to determine, separately, the full-span value of lift coefficient increments appropriate to the flap deflection and flap-chord to wing-chord ratios of the inner and outer panels at the Reynolds number of interest. The part-span correction method in Item No. 74012 (Derivation 34) is then applied to reduce the full-span coefficients to the values appropriate to the spanwise extent of each panel. Note that the inner panel has a fictitious inboard extension added to account theoretically for body interference, as described in Item No. 75013 (Derivation 35). For an angle of attack of $\alpha = 6°$ those procedures give a lift coefficient of 0.369 for the inner panel and 0.356 for the outer panel, giving a total increment $\Delta C_{Lf} = 0.725$. The flap system considered in the example extends the local wing chord and therefore ΔC_{Lf} varies with α, but this variation is only about 10 per cent as α varies between 0 and 10° and for the purposes of the present example ΔC_{Lf} has been assumed to remain constant at its value for $\alpha = 6°$.

The flap lift coefficient increments are summarised in Table 5.4.

TABLE 5.4 Flap Lift Coefficient Increments

Parameter	*Landing Configuration (flaps deployed)*		
	Inner flap panels	*Outer flap panels*	*Total*
ΔC_{Lf}	0.369	0.356	0.725

The total lift coefficient of the wing at $M = 0.20$ with flaps deployed is therefore

$C_L = 0.0782(\alpha + 3) + 0.725$. At $\alpha = 6°$ this gives $C_L = 0.704 + 0.725 = 1.429$.

5.2.3 Total Lift Coefficient

It is sometimes desirable to plot the stability derivatives against total C_L rather than angle of attack. In the present example, sufficiently accurate values of C_L are obtained for this by using values for the wing alone and for the wing with flaps deployed. No contribution is estimated for the tailplane since this is relatively small compared to the wing value; the minor contributions from the body and nacelles are also neglected. For other aircraft configurations, where the tail surface is large compared to the wing or where the body or nacelles provide a substantial part of the lift, their contributions should be included where possible.

The total lift for the cruise configuration is thus approximated by

$$C_L = (5.69/57.3)(\alpha + \alpha_w) = 0.0993(\alpha + 3), \tag{5.1}$$

and for the landing configuration by

$$C_L = (4.48/57.3)(\alpha + \alpha_w) + \Delta C_{Lf} = 0.0782(\alpha + 3) + 0.725. \tag{5.2}$$

5.3 Calculation of Wing Planform Contributions, $(Y_p)_w$, $(N_p)_w$ and $(L_p)_w$

5.3.1 Sideforce and yawing moment contributions, $(Y_p)_w$ and $(N_p)_w$

See Item No. 81014 for Notation.

The values of $(Y_p)_w$ and $(N_p)_w$ are estimated using Item No. 81014. In that Item the incompressible flow values of the initial linear variations with C_L, $[(Y_p)_w/C_L]_O$ and $[(N_p)_w/C_L]_O$, are predicted largely on the basis of strip theory and simple lifting-line considerations, with empirical corrections added to allow for the presence of wing edge forces. Those parameters are functions of the wing aspect ratio, A, and sweep, $\Lambda_{¼}$, and $(N_p)_w$ also depends on the distance of the wing aerodynamic centre aft of the moment reference centre, x_{ac}. For $(N_p)_w$ the Item contains an empirical modification, $\Delta(N_p)_w$, that models the non-linear variation of N_p as the edge forces decay (see Section 3.2). The successful application of that modification requires a good knowledge of the rate of change of the viscous drag coefficient with α, *i.e.* $\partial C'_D/\partial\alpha$ where $C'_D = C_D - C_L^2/\pi A$. In Item No. 81014, $\Delta(N_p)_w/(\partial C'_D/\partial\alpha)$ is given as a function of $\Lambda_{¼}$ and A. For this example the values of $\partial C'_D/\partial\alpha$ in Table 5.5 are assumed.

To allow for compressibility effects Item No. 81014 gives correction factors $[(Y_p)_w/C_L]_M/[(Y_p)_w/C_L]_O$ and $[(N_p)_w/C_L]_M/[(N_p)_w/C_L]_O$, where $[\ ]_M$ denotes values at a Mach number M. The factors are presented in a series of carpets depending on M, $\Lambda_{¼}$ and A.

The values of the parameters involved in calculating $(Y_p)_w$ and $(N_p)_w$ are set out in Table 5.6.

The method in Item No. 81014 can be adapted to deal approximately with high-lift devices by substituting the values of C_L and C_D appropriate to those configurations. This procedure is recommended in Reference 28 which states that comparisons with experimental data have indicated that reasonably good estimates can be expected.

TABLE 5.5 Values of $\partial C'_D/\partial\alpha$ Assumed in Example

α	–2°	0	2°	4°	6°	8°	10°
Cruise Conditions	0	0.0006	0.0015	0.0029	0.0050	–	–
Landing Conditions Flaps Deployed	0	0.0004	0.0009	0.0017	0.0028	0.0042	0.0079
Landing Conditions Flaps Restracted	0	0.0001	0.0004	0.0008	0.0012	0.0017	0.0023

TABLE 5.6 Calculation of $(Y_p)_w$ and $(N_p)_w$

Parameter	*Cruise configuration*	*Landing configuration*
α	0	6°
M	0.78	0.20
A	7.59	7.59
$\Lambda_{¼}$	28.6°	28.6°
x_{ac}/b	0	0
$[(Y_p)_w/C_L]_O$	0.275	0.275
$[(N_p)_w/C_L]_O$	–0.047	–0.047
$\Delta(N_p)_w/(\partial C_D'/\partial\alpha)$	2.7	2.7
$\dfrac{[(Y_p)_w/C_L]_M}{[(Y_p)_w/C_L]_O}$	0.93	1.0
$\dfrac{[(N_p)_w/C_L]_M}{[(N_p)_w/C_L]_O}$	0.90	1.0
C_L	0.298	1.429
$\partial C_D'/\partial\alpha$	0.0006	0.0028
$(\Delta N_p)_w$	0.0015	0.0076
$(Y_p)_w$	0.076	0.393
$(N_p)_w$	–0.011	–0.060
$(Y_p)_w$ as a function of α	$0.0254(\alpha+3)$	$0.0215(\alpha+3)+0.199^*$
$(N_p)_w$ as a function of α	$-0.00420(\alpha+3)+2.43\partial C_D'/\partial\alpha$	$-0.00367(\alpha+3)-0.0341^*+2.7\partial C_D'/\partial\alpha$
*Contributions due to flap lift increment ΔC_{Lf}		

5.3.2 Rolling moment contribution, $(L_p)_w$

See Item No. Aero A.06.01.01 for Notation.

The wing planform contribution $(L_p)_w$ is obtained from Item No. Aero A.06.01.01 which contains results derived from simplified lifting-surface theory. In that Item the quantity $\beta L_p/\kappa$ is presented graphically as a function of $\beta A/\kappa$, Λ_E and λ, where $\beta = (1-M^2)^{½}$, $\kappa = \beta(a_{10})_M/2\pi$, $\Lambda_E = \tan^{-1}([\tan\Lambda_{¼}]/\beta)$ and $(a_{10})_M$ is the two-dimensional lift-curve slope of the wing section at the Mach number and Reynolds number of interest.

The value of $(L_p)_w$ obtained from Item No. Aero A.06.01.01 is independent of α but it is known that at high angles of attack the experimental values of $(L_p)_w$ decrease in magnitude and may eventually become positive due to the occurrence of flow separation. A limit of applicability of $C_L = 0.5$ is given in the Item. However, Derivation 27 extends the theoretical result that $(L_p)_w$ depends on the wing lift-curve slope a_1 to the approximation that flow separation will influence $(L_p)_w$ to the same degree that it influences a_1. The validity of this is demonstrated in Derivation 27 for a variety of wing planforms for which experimental values of $(L_p)_w$ and a_1 are available. Therefore, when a_1 ceases to vary linearly, $(L_p)_w$ can be corrected through the equation

$$(L_p)_w = [(L_p)_w]_{\text{A.06.01.01}}[a_1/(a_1)_{C_{L=0}}], \tag{5.3}$$

where $[(L_p)_w]_{\text{A.06.01.01}}$ is the value obtained from Item No. Aero A.06.01.01 and $(a_1)_{C_{L=0}}$ denotes the linear value of a_1 at low incidence. The correction provided by Equation (5.3) requires experimental values of a_1 but it is seldom needed.

It may be noted that Derivation 27 also considers a more detailed correction to $(L_p)_w$. In addition to the right-hand side of Equation (5.3) this incorporates small contributions from the profile drag and the induced drag. Comparisons with experimental data show that these lead to only a marginal improvement over Equation (5.3) and may be ignored within the likely tolerance on the prediction of $(L_p)_w$ at high α.

The deployment of high-lift devices is not treated in Item No. Aero A.06.01.01. However, they should not greatly change the section lift-curve slope $(a_{10})_M$. Therefore the clean-wing values of $(L_p)_w$ should still provide satisfactory estimates below the stall. This has been substantiated by comparisons with the small number of relevant experimental data that are available (Derivations 5, 6, 17 and 25). The main effect of the high-lift devices is to extend the range of α over which the lift coefficient varies linearly. As would be expected from Equation (5.3), this is reflected by a corresponding increase in the range over which the experimental values of $(L_p)_w$ remain constant.

For the purpose of the present example $(L_p)_w$ is estimated solely from Item No. Aero A.06.01.01. The values of the parameters involved are set out in Table 5.7.

TABLE 5.7 Calculation of $(L_p)_w$

Parameter	*Cruise Configuration*	*Landing Configuration*
α	0	6°
M	0.78	0.2
β	0.626	0.980
$(a_{10})_M$	8.44	6.23
κ	0.841	0.972
$\beta A/\kappa$	5.65	7.65
Λ_E	41.1°	29.1°
λ	0.246	0.246
$-\beta(L_p)_w/\kappa$	0.170	0.206
$(L_p)_w$	–0.228	–0.204

5.4 Calculation of Wing Dihedral Contributions, $(Y_p)_\Gamma$, $(N_p)_\Gamma$ and $(L_p)_\Gamma$

See Item No. 85006 for Notation.

The contributions of the wing dihedral are calculated from the results given in Item No. 85006. Those results are derived from strip-theory and lifting-line considerations. The derivatives are each given in terms of the wing planform contribution $(L_p)_w$ and depend on Γ, A, $\Lambda_{¼}$ and λ. The quantity $(N_p)_\Gamma$ also involves the distance of the moment reference centre ahead of the wing aerodynamic centre, ξs, and the perpendicular distance of the wing root chord below the moment reference centre, ζs. The derivatives $(Y_p)_\Gamma$ and $(L_p)_\Gamma$ depend on ζ but not ξ. For sideforce, $(Y_p)_\Gamma$ is given in both graphical and mathematical forms since it can provide a large contribution to Y_p. The small contributions $(N_p)_\Gamma$ and $(L_p)_\Gamma$, are only given mathematically. Simplified expressions corresponding to $\sin\Gamma \approx \Gamma/57.3$, $\zeta = 0$ and $\lambda = 1/3$ are also given in the Item. These suffice for $(N_p)_\Gamma$ and $(L_p)_\Gamma$. The full expression for $(Y_p)_\Gamma$ is preferred in this example although, in practice, the simplified expression will often prove adequate. The parameters involved in the calculation are set out in Table 5.8.

TABLE 5.8 Calculation of $(Y_p)_\Gamma$, $(N_p)_\Gamma$ and $(L_p)_\Gamma$

Parameter	*Cruise Configuration*	*Landing Configuration*
α	0	6°
M	0.78	0.2
ξ	0	0
ζ	0.057	0.057
Γ	3°	3°
A	7.59	7.59
$\Lambda_{¼}$	28.6°	28.6°
λ	0.246	0.246
$(Y_p)_\Gamma/(L_p)_w$	0.178	0.178
$(N_p)_\Gamma/(L_p)_w$	–0.009	–0.009
$(L_p)_\Gamma/(L_p)_w$	–0.010	–0.010
$(L_p)_w$	–0.228	–0.204
$(Y_p)_\Gamma$	–0.041	–0.036
$(N_p)_\Gamma$	0.002	0.002
$(L_p)_\Gamma$	0.002	0.002

5.5 Additional Wing Contributions, $(N_p)_\varepsilon$ and $(N_p)_f$

In addition to the contributions described in Sections 5.3 and 5.4, strip-theory calculations are used in Derivation 26 to show that there are theoretical contributions to the yawing moment derivative due to wing twist and due to flap deployment at constant C_L. Those contributions, $(N_p)_\varepsilon$ and $(N_p)_f$, are estimated in Derivation 26 by dividing the spanwise distribution of the angle of attack on a rolling wing into a part that is proportional to C_L and another that is proportional to linear twist or to flap deflection angle alone. The influence of the former part is automatically incorporated into the wing planform component $(N_p)_w$. The contributions $(N_p)_\varepsilon$ and $(N_p)_f$ from the latter part can be estimated by means of Derivation 26, but their magnitudes are generally too small to be of any significance and they are omitted from this example. In particular the flap contribution $(N_p)_f$ is likely to be far less important than the influence of the flap lift coefficient increment on $(N_p)_w$.

5.6 Calculation of Fin and Tailplane Contributions, $(Y_p)_F$, $(N_p)_F$, $(L_p)_F$ and $(L_p)_T$

See Item No. 83006 for Notation.

The contributions $(Y_p)_F$, $(N_p)_F$ and $(L_p)_F$ are calculated from the method contained in Item No. 83006. The basis of the method is that the theoretical contribution of an isolated fin-tailplane arrangement is modified to incorporate empirical corrections that allow for the rolling sidewash field caused by the presence of the wing and the body. The equations given in that Item are

$$(Y_p)_F = -(K_1 + K_2K_3)\frac{S_F h_F}{S_W b}\left\{\frac{(\overline{z_F^*}\cos\alpha - \overline{l_F^*}\sin\alpha)/b - \partial\bar{\sigma}_W/\partial(pb/V) - \partial\bar{\sigma}_\alpha/\partial(pb/V)}{(\overline{z_F^*} - z_{crF})/b}\right\}, \tag{5.4}$$

$$(N_p)_F = -(Y_p)_F(\overline{l_F^*}\cos\alpha + \overline{z_F^*}\sin\alpha)/b, \tag{5.5}$$

and

$$(L_p)_F = (Y_p)_F(\overline{z_F^*}\cos\alpha - \overline{l_F^*}\sin\alpha)/b, \tag{5.6}$$

The functions K_1, K_2 and K_3 are given graphically in Item No. 83006 as functions of fin aspect ratio, A_F, quarter-chord sweep, $\Lambda_{¼F}$, tailplane span to fin height, b_T/h_F, and tailplane height to fin height, z_T/h_F. They arise from the theoretical calculation for the isolated fin-tailplane arrangement. The function K_1 allows for the basic isolated fin damping and K_2 and K_3 model the interference effect of the tailplane. The centre of pressure of the fin loading is evaluated in terms of the fin moment arms $\overline{z_F^*}$ and $\overline{l_F^*}$ that are measured normal and parallel to the body longitudinal axis. They are expressed in terms of the height of the fin root chord above the body longitudinal axis, z_{crF}, and the distance of the fin root quarter-chord point aft of the moment reference centre, m_F, *i.e.*

$$\overline{z_F^*} = z_{crF} + \{0.5h_F + 0.2\,|z_T - 0.5h_F|\} \tag{5.7}$$

and

$$\overline{l_F^*} = m_F + \{0.5h_F + 0.2\,|z_T - 0.5h_F|\}\tan\Lambda_{¼F}, \tag{5.8}$$

where z_T is the tailplane height on the fin. For body-mounted tailplanes the substitution $z_T = 0$ gives the appropriate values of $\overline{z_F^*}$ and $\overline{l_F^*}$. The vertical and longitudinal moment arms in stability axes are $(\overline{z_F^*}\cos\alpha - \overline{l_F^*}\sin\alpha)$ and $(\overline{l_F^*}\cos\alpha + \overline{z_F^*}\sin\alpha)$. The influence of these distances is clear in Equations (5.4) to (5.6).

The term $\partial\bar{\sigma}_W/\partial(pb/V)$ appears in Equation (5.4) to allow for the mean sidewash induced at the fin by the rolling wing. The comparisons made with a large number of experimental values of the fin contributions during the development of Item No. 83006 demonstrated that this sidewash parameter could be assumed to be independent of the angle of attack, at least for $0 \le \alpha \le 15°$, and that good overall accuracy was achieved if a constant value of 0.18 was taken. Attempts to allow for a variation with aircraft geometry by determining $\partial\bar{\sigma}_W/\partial(pb/V)$ empirically, or by representing the wake of the rolling wing by a system of trailing horseshoe vortices did not lead to any general improvement in prediction. The horseshoe vortex model predicts values that are far too low for direct use in Equation (5.4). Nevertheless, it does provide qualitative support for the adoption of a simple constant value by revealing that for practical configurations the sidewash parameter is largely unaffected by the distance of the fin downstream of the wing, the wing sweep or the wing taper. There is a reduction in the predicted sidewash parameter as the wing aspect ratio increases and an increase

as the ratio of the fin height to wing span falls. For geometries of interest there is a tendency for these two opposing effects to cancel, so that $\partial\bar{\sigma}_W/\partial(pb/V)$ varies relatively little from configuration to configuration.

The other term $\partial\bar{\sigma}_\alpha/\partial(pb/V)$ in Equation (5.4) varies with α and represents the presence of body sidewash and any decrease in fin effectiveness that results as α increases. It is presented in graphical form in Item No. 83006 as a function of the parameter $[\bar{z}_F^* - (\bar{z}_F^* \cos\alpha - \bar{l}_F^* \sin\alpha)]/b$.

In addition to the fin contribution treated above, there is a tailplane planform contribution to the rolling moment, $(L_p)_T$. Because of the rotation of the flow caused by the wing this is equal to only half the value of $(L_p)_w$ that would be estimated for an isolated tailplane, so that,

$$(L_p)_T = 0.5(L_p)_w S_T b_T^2 / Sb^2, \tag{5.9}$$

where $(L_p)_w$ is calculated as in Section 5.3.2 with parameters appropriate to the tailplane.

The values of the parameters involved in the calculation of the fin and tailplane contributions are set out in Table 5.9.

It should be noted that the fin contributions are strongly affected by the sidewash, which is usually so large that it changes the sign of the contributions. For instance, at $\alpha = 0$ and in the absence of sidewash Equations (5.4) to (5.6) give $(Y_p)_F = -0.049$, $(N_p)_F = 0.023$ and $(L_p)_F = -0.008$. These compare with the values $(Y_p)_F = 0.017$, $(N_p)_F = -0.008$ and $(L_p)_F = 0.003$ for the case where sidewash is present. Because of this and the difficulty of estimating the sidewash reliably the effect of variations should be considered. For the aircraft of this example changes of ± 20 per cent in the sidewash cause changes of ± 0.01 in $(Y_p)_F$, ± 0.005 in $(N_p)_F$ and ± 0.002 in $(L_p)_F$. In particular the change in $(N_p)_F$ can be a significant proportion of N_p.

As the deployment of high-lift devices causes a symmetric change to the wing loading the effect on the fin contributions should be small. There will however be a change in the downwash field and this will have a secondary influence on the sidewash. Therefore, slightly higher tolerances should be considered in such cases.

TABLE 5.9 Calculation of $(Y_p)_F$, $(N_p)_F$ and $(L_p)_T$

Parameter	*Cruise Configuration*	*Landing Configuration*
α	0	6°
M	0.78	0.20
A_F	2.10	2.10
$\Lambda_{¼F}$	43.0°	43.0°
b_T/h_F	2.46	2.46
z_T/h_F	0.587	0.587
$h_F S_F/Sb$	0.0319	0.319
K_1	0.81	0.81
K_2	0.22	0.22
K_3	0.05	0.05
z_{crF}/b	0.0755	0.0755
m_F/b	0.391	0.391
$\overline{z_F^*}/b$	0.160	0.160
$\overline{l_F^*}/b$	0.470	0.470
$(Y_p)_F$	0.006	0.044
$(N_p)_F$	–0.003	–0.021
$(L_p)_F$	0.001	0.005
$(L_p)_w$(tailplane)	–0.113	0.136
$0.5S_T b_T^2/Sb^2$	0.0234	0.0234
$(L_p)_T$	–0.003	–0.003

The variation of the fin contribution with α is

α	–2°	0	2°	4°	6°	8°	10°
$(Y_p)_F$	–0.006	0.006	0.018	0.031	0.044	0.058	0.072
$(N_p)_F$	0.003	–0.003	–0.009	–0.015	–0.021	–0.028	–0.035
$(L_p)_F$	–0.001	0.001	0.003	0.004	0.005	0.005	0.006

5.7 Summary of Results and Total Values

The results of the calculations of the various component parts of Y_p, N_p and L_p are summarised in Table 5.10 and illustrated in Sketches 5.2 and 5.3 for the cruise $(\alpha = 0)$ and landing $(\alpha = 6°)$ conditions respectively. The variations of the part and total derivatives with α and C_L are shown in Sketches 5.4 and 5.5.

For the cruise configuration it can be seen that at low α the derivative Y_p is determined by the opposing wing dihedral and wing planform contributions, with the latter increasing and dominating at high α, where the fin contribution is also becoming significant. But note that in practice $(Y_p)_w$ will reduce as the wing edge forces decay, see Section 3.2.1.

At low α the derivative N_p is made up of small contributions from the wing dihedral, wing planform and fin. As α increases the planform and fin contributions increase and together determine N_p. See Section 3.2 for a discussion of how edge forces influence the variation of $(N_p)_w$.

The wing planform contribution completely dominates L_p, which is essentially independent of α. But refer to the comments in Sections 3.2.1 and 5.3.2 on the reduction in the magnitude of L_p that is to be expected in practice at high α and to Section 3.2.4 where an increase in magnitude is found in the case of high sweep angle.

Sketches 5.3 and 5.5 show that the effect of flap deployment is to increase the magnitudes of the wing planform contributions to Y_p and N_p because of the increase in C_L. There is no effect on the predicted value of L_p.

TABLE 5.10 Calculation of Total Values

Parameter	*Cruise Configuration*	*Landing Configuration*
α	0	6°
M	0.78	0.20
$(Y_p)_w$	0.076	0.393
$(Y_p)_\Gamma$	–0.041	–0.036
$(Y_p)_F$	0.006	0.044
Y_p	0.041	0.401
$(N_p)_w$	–0.011	–0.060
$(N_p)_\Gamma$	0.002	0.002
$(N_p)_F$	–0.003	–0.021
N_p	–0.012	–0.079
$(L_p)_w$	–0.228	–0.204
$(L_p)_\Gamma$	0.002	0.002
$(L_p)_F$	0.001	0.005
$(L_p)_T$	–0.003	–0.003
L_p	–0.228	–0.200

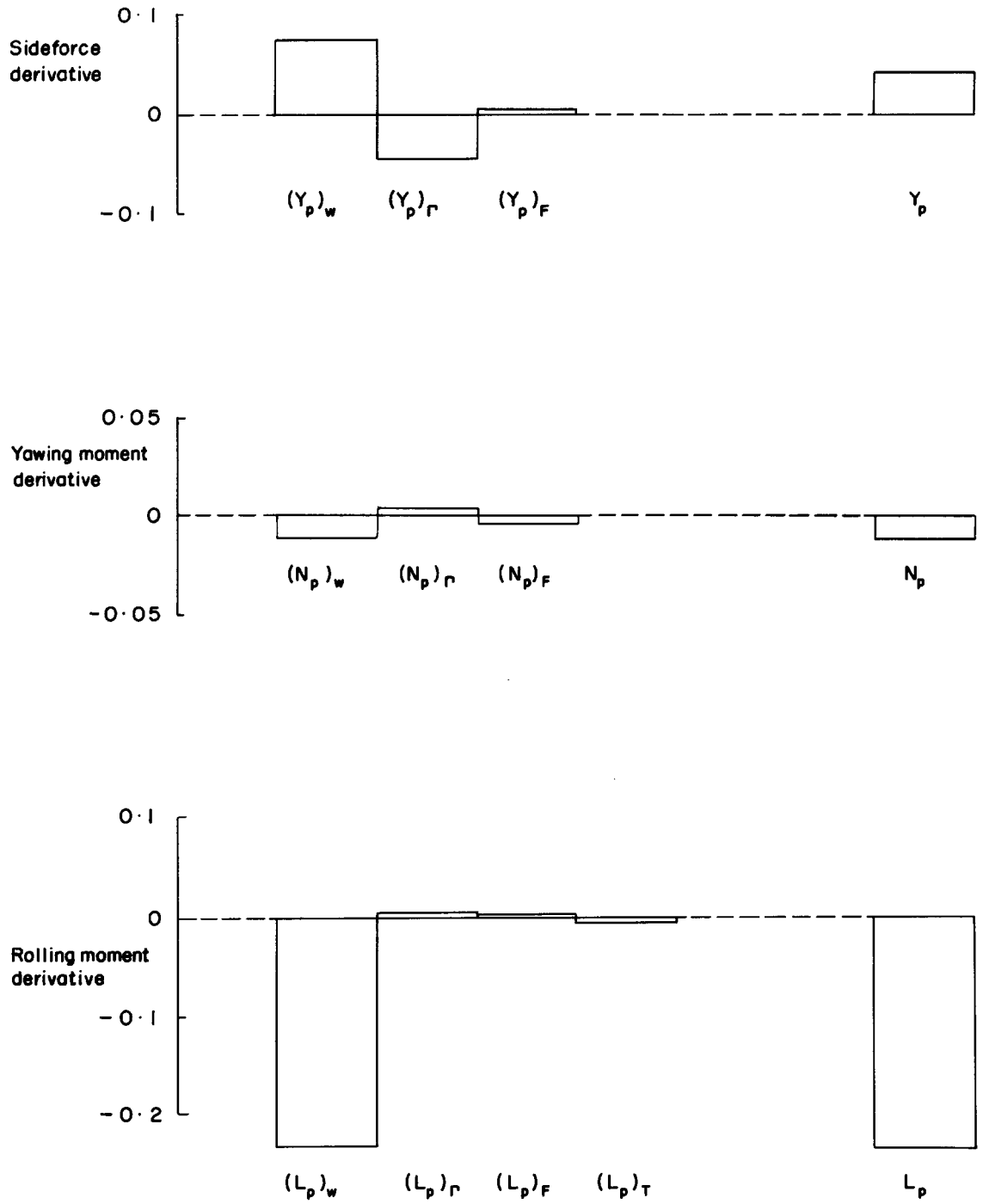

Sketch 5.2 Comparison of components for cruise configuration, $\alpha = 0$

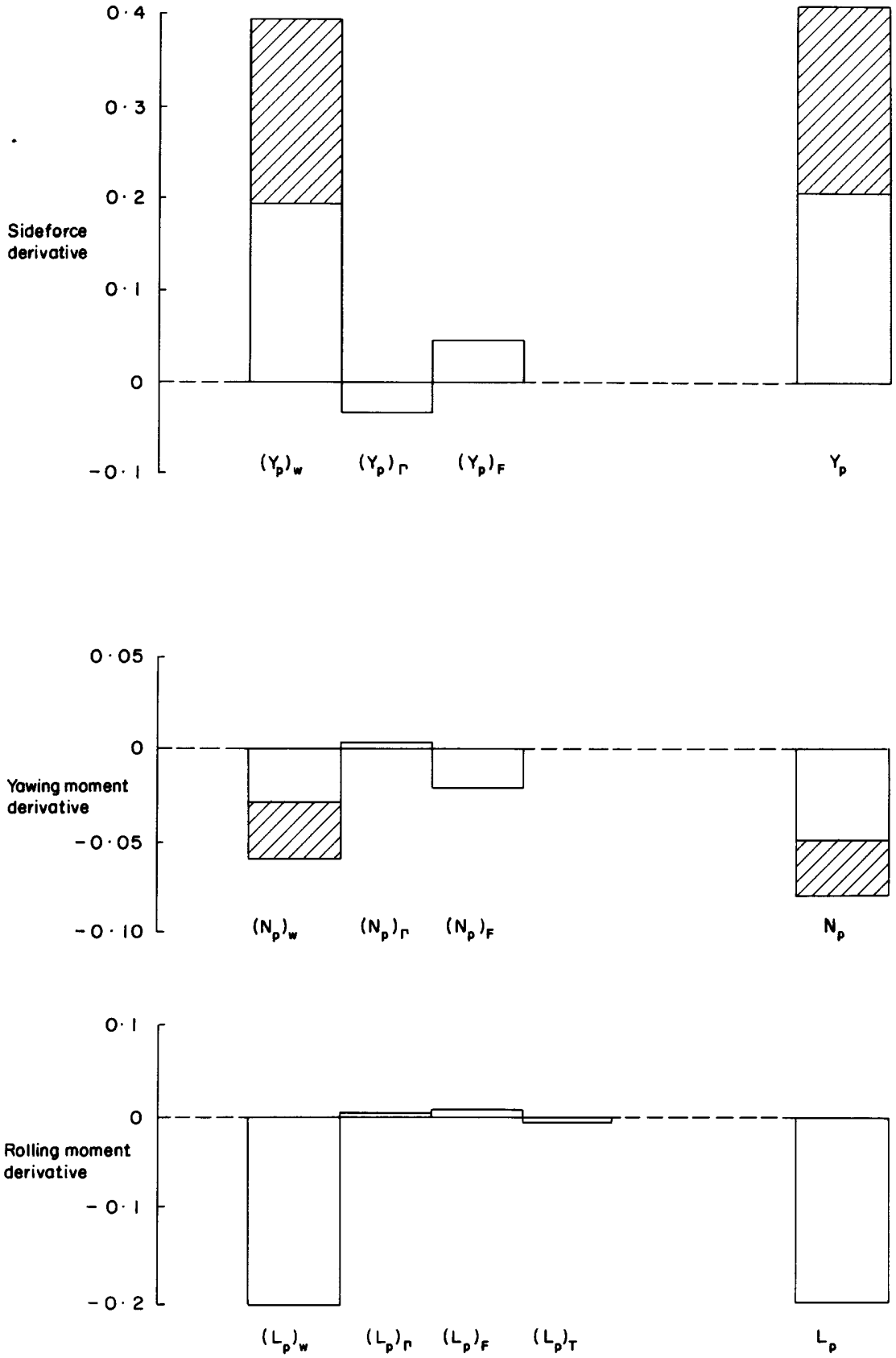

Sketch 5.3 Comparison of components for landing configuration, $\alpha = 6°$ (shaded areas show difference between flaps-deployed and flaps-retracted values)

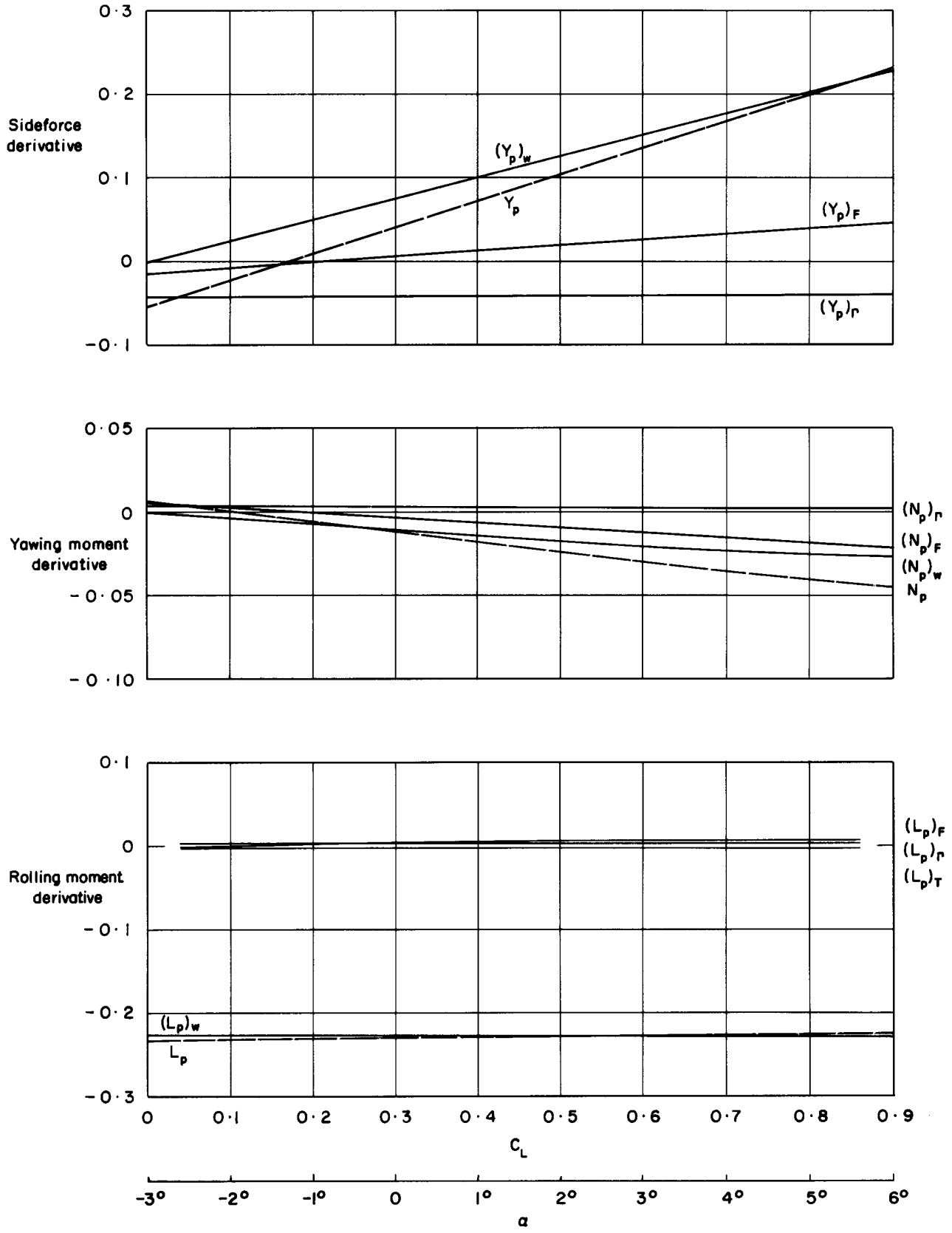

Sketch 5.4 Variation with α and C_L of part and total derivatives for cruise configuration, $M = 0.78$

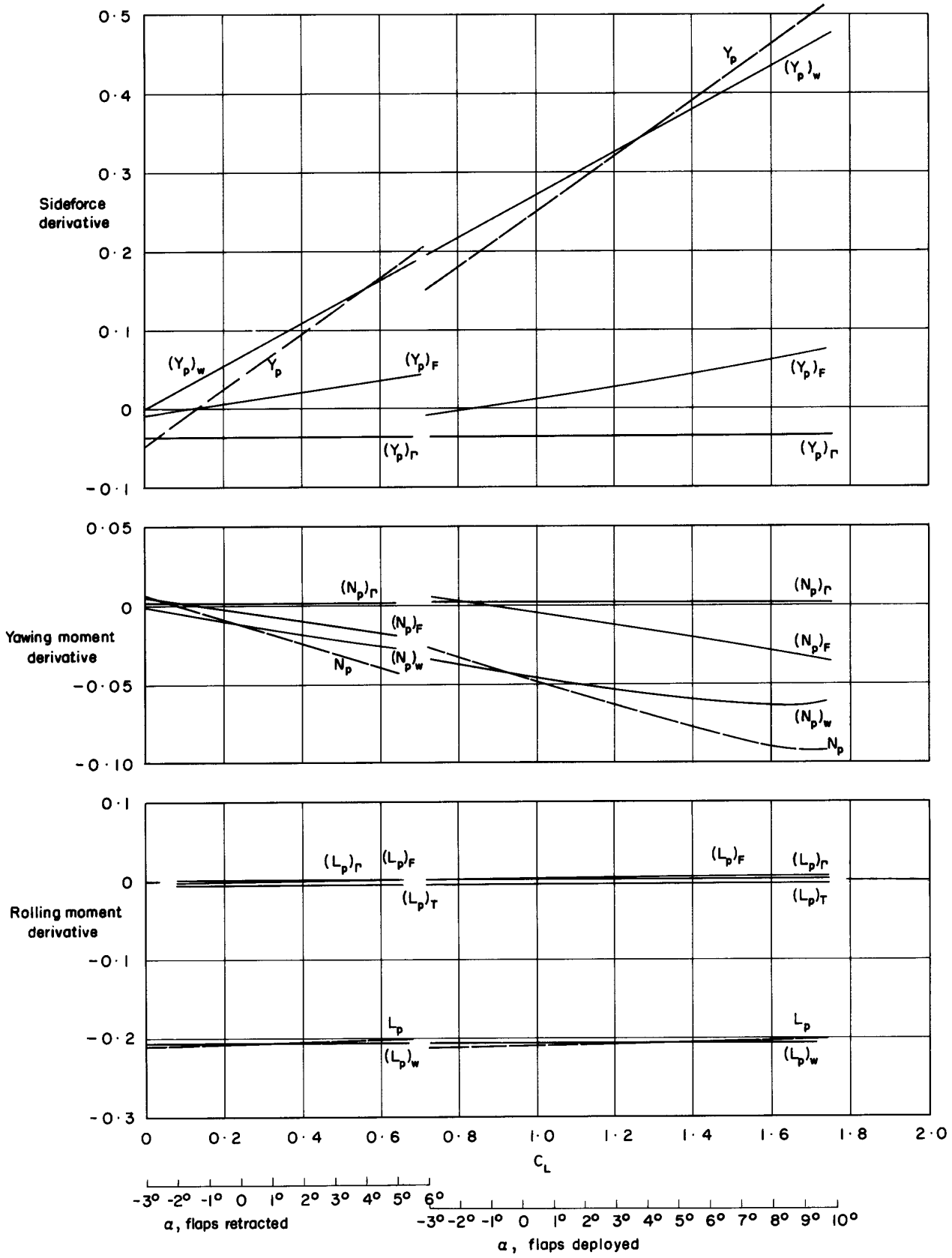

Sketch 5.5 Variation with α and C_L of part and total derivatives for landing configuration, $M = 0.2$

THE PREPARATION OF THIS DATA ITEM

The work on this particular Item was monitored and guided by the Aerodynamics Committee which first met in 1942 and now has the following membership:

Chairman

Mr H.C. Garner	–	Independent

Vice-Chairman

Mr P.K. Jones	–	British Aerospace, Aircraft Group, Manchester

Members

Mr D. Bonenfant	–	Aérospatiale, Toulouse, France
Mr E.A. Boyd	–	Cranfield Institute of Technology
Mr K. Burgin	–	Southampton University
Mr E.C. Carter	–	Aircraft Research Association
Mr J.R.J. Dovey		British Aerospace, Aircraft Group, Warton
Dr J.W. Flower	–	Bristol University
Mr A. Hipp	–	British Aerospace, Dynamics Group, Stevenage
Mr J. Kloos*	–	Saab-Scania, Linköping, Sweden
Mr J.R.C. Pedersen	–	Independent
Mr I.H. Rettie*	–	Boeing Aerospace Company, Seattle, Wash., USA
Mr R. Sanderson	–	Messerschmitt-Bölkow-Blohm GmbH, Hamburg, W. Germany
Mr A.E. Sewell*	–	Northrop Corporation, Hawthorne, Calif., USA
Mr F.W. Stanhope	–	Rolls-Royce Ltd, Derby
Mr H. Vogel	–	British Aerospace, Aircraft Group, Weybridge.

* Corresponding Member

The member of staff who undertook the technical work involved in the initial assessment of the available information and the construction and subsequent development of the Item was

Mr R.W. Gilbey	–	Senior Engineer.